ACS Catalysis

pubs.acs.org/acscatalysis
Research Article

Microkinetic Assessment of Ligand-Exchanging Catalytic Cycles

Orkhan Abdullayev, Diego Garay-Ruiz,* Berta Bori-Bru, and Carles Bo*

Cite This: ACS Catal. 2025, 15, 4739–4745
Read Online

ACCESS | Metrics & More | Article Recommendations | Supporting Information

ABSTRACT: Computational chemistry has become a fundamental part of the understanding and optimization of catalytic processes. Among these, the characterization of homogeneous organometallic catalysts, combining an active transition metal atom and set of ligands, is one of the main fields of application of these kinds of studies. More recently, microkinetic studies have been employed to bridge the gap between experimental measurements such as conversion or selectivity and the Gibbs free energies gathered by computations. In this work, we have developed an automated framework (MicroKatc) for microkinetic analysis, to tackle the yet understudied effect of ligand exchange processes that modify the nature of the catalytic scaffold *in situ*. We report the application of such a framework to the rhodium-catalyzed hydroformylation of ethylene, confirming the acceleration of the reaction as trimethylphosphine (PMe_3) displaces the carbonyl ligands in the catalyst by means of simulations at variable phosphine concentrations, as well as the determination of the degree of rate control (DRC) and apparent activation energies throughout the catalytic process.

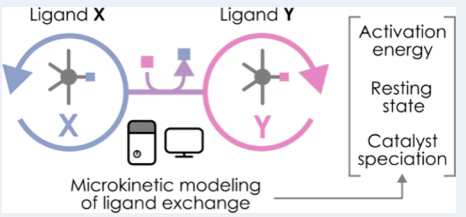

KEYWORDS: *microkinetic modeling, hydroformylation, homogeneous catalysis, DFT, reaction network, catalytic cycles*

INTRODUCTION

Computational chemistry has become an essential tool for the study of catalytic processes, both in the homogeneous[1−10] and heterogeneous[11−15] phases. The characterization of reaction mechanisms by means of Density Functional Theory (DFT) enables a deeper understanding of how these complex processes actually take place with the goal of eventually fine-tuning and optimizing the catalyst. The traditional approach to such studies regarded the direct inspection of the energy profiles associated with the catalytic process, identifying the global thermodynamic and kinetic trends associated with the mechanism. However, the wide availability of more powerful computers has deeply increased the degree of detail in which these chemical processes are described and thus their subsequent complexity. In this sense, mechanism elucidation produces Chemical Reaction Networks (CRNs) that can be strongly interconnected and therefore cannot be summarized as linear free energy profiles. This is even more relevant under the framework of automated mechanism discovery algorithms,[16−22] whose size and interconnectivity tend to be even larger. Then, it becomes essential to employ tools that consider the complete picture of the complex CRN to extract chemical information. As a first example, we may consider the well-known energy span model (ESM) from Kozuch and coworkers,[23,24] which was reformulated[25] and reimplemented[26] to handle these kinds of reaction networks. Moreover, the use of microkinetic modeling, which once was mostly oriented to heterogeneous catalysis,[27−30] has now become more of a standard tool for homogeneous systems.[31−37]

Putting the focus on homogeneous catalysis, an essential feature of this kind of system is the importance of the *ligands* that bind to the metal center. Even when these ligands are not directly involved in the reaction, their role on tuning the electronic and steric properties of the complex marks the efficacy and selectivity of the catalyzed reaction.[38−41] While it is common to evaluate the effect of different ligands in the reactivity of a complex, both experimentally[42−44] and computationally,[45−49] it is not as usual to explore how *in situ* ligand exchange (e.g., by addition of a competitive ligand) may affect the performance of the system. Nonetheless, taking into account this ligand exchange implies the characterization of connected catalytic cycles bearing one or the other ligand (Figure 1), whose analysis is far from trivial. In this toy example, a catalytic system with the net reaction A + B → C is illustrated, with ligands L_x and L_y being exchanged.

Initially, we aimed to apply the CRN-based energy span model (ESM) to explore such systems, employing our previously reported implementation: gTOFfee.[26,50] However, the ESM encounters important issues when dealing with this specific kind of connected catalytic cycle, which prevented us from proceeding with this approach. Specifically, in situations like the one showcased in Figure 1, it is key to properly control the individual concentrations of the catalyst-bearing species in all the possible forms of the catalyst (here, X and Y), which depend on the initial amount of L_x and L_y ligands in the

Received: January 14, 2025
Revised: February 19, 2025
Accepted: February 19, 2025
Published: March 6, 2025

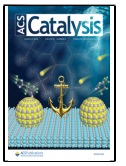

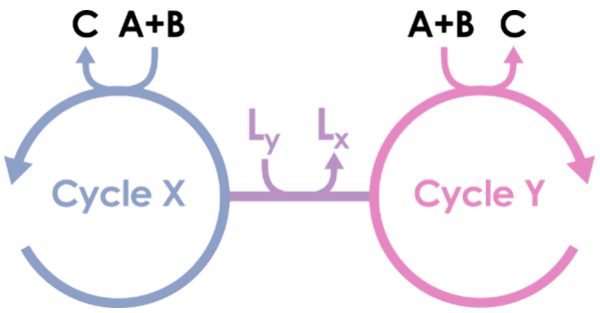

Figure 1. Schematic depiction of ligand-exchange-connected catalytic cycles X and Y.

medium. As concentration effects in the ESM are based on the semi-standard state approximation that does not consider the individual concentrations of the catalyst-bearing species, this bifurcation cannot be properly treated.

Therefore, we resorted to microkinetic modeling, which explicitly handles *all* concentrations in the system. These simulations provide an ideal platform to study this kind of system, enabling one to tweak the initial concentrations of both the catalyst and competing ligands to gather the complete picture.

METHODOLOGY

To properly explore the influence of ligand exchange processes on the overall activity of catalytic systems, it is essential to *automate* the generation and resolution of these models. Several automation drivers have been reported in the literature although with a focus on heterogeneous catalysis, such as CaRMeN[51] or AMUSE.[52]

To do that, we developed a new automation platform, named MicroKatc, which streamlines not only the setup but also the analysis of the numerous results that are generated.

The very first step of the procedure (Figure 2) is the DFT characterization of the Gibbs free energies of the target

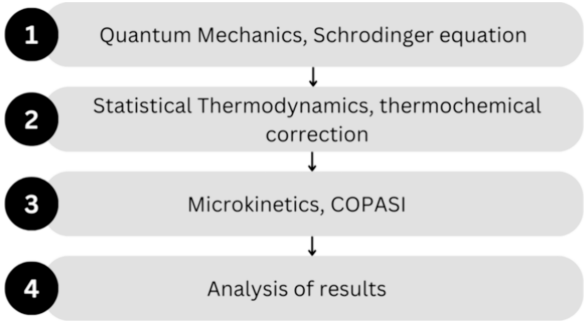

Figure 2. Basic workflow of MicroKatc.

reaction mechanism with external QM software, defining all possible species and chemical reactions. It is worth noting that, for the case of processes considered as barrierless (i.e., not having an associated transition state), they should be considered as diffusion-controlled.[31] Once all species have been characterized, the corresponding output files must be collected and passed to MicroKatc. Afterward, the reference state employed to compute the thermochemical parameters should be corrected: while QM calculations most often consider a reference state of 298.15 K and 1 atm (gas phase), proper microkinetic simulations in solution require a 1.0 M reference state, as well as the consideration of the actual working temperature. To do this, the *thermochange*[53] package was interfaced with MicroKatc. This utility handles the parsing of the output files, currently supporting Gaussian (as employed in the working example) and ADF, as well as the recalculation of the corresponding partition functions and thermodynamic potentials. In this way, MicroKatc extracts and corrects the energetic information automatically from the raw output files. Nonetheless, it is also possible to bypass this parsing step and employ a CSV file containing the names and free energies of all of the involved molecules.

The other main piece of input required by the program is the definition of the chemical reactions that interlink the corresponding species to set up the microkinetic model. This information is supplied as a plain text file, where each reaction is defined as a string of the form A + B = C for the reversible reaction A + B ⇄ C. For irreversible reactions, the "->" symbol might be used instead of the equal sign. As a solver, we have employed COPASI.[54] To simplify the integration with computational chemistry results, we have developed the *copasi-helper* package.[55] From the aforementioned list of reaction definitions and the energies extracted from the outputs, MicroKatc computes the direct and reverse barriers for all reactions to determine the rate constants, completing the setup of the model as a system of differential equations that COPASI can solve.

From here, several possible variations on the target microkinetic model can be produced and analyzed. First and foremost, the comparison of the catalytic performance of models with varying initial concentrations of the ligand whose exchange is under study is streamlined by running the already defined models under different sets of initial parameters. Moreover, it is also possible to set up simulations in a range of temperatures, enabling the study of apparent activation energies (E_a^{app}) through an Arrhenius-like rate law. At these varying temperatures, MicroKatc automatically recomputes Gibbs free energies and rate constants and performs the microkinetic simulation. Then, parameters of choice, such as reaction rates, can be extracted and plotted.

Other major feature of the code is the systematic perturbation of the reaction barriers to determine the degree of rate control (DRC)[56] of all elementary reactions in the mechanism. For each reaction in the system, the direct and reverse barriers are modified by a fixed amount, determining how strongly the reaction rate is affected by this perturbation. Again, MicroKatc streamlines the automated application of this procedure not only to a fixed set of initial conditions but also to explore variations upon them: for instance, as studied in this work, a range of initial ligand concentrations.

Throughout these tools, which have been scarcely applied to homogeneous catalysis, it is possible to gather deep insights into the studied systems with minimal user effort. In the following section, we will discuss the very well-known Rh-catalyzed hydroformylation reaction, with CO and PMe_3 as ligands, as a test example for our new simulation platform.

Application. Hydroformylation is, to our knowledge, the most relevant industrial application of homogeneous transition metal-catalyzed[57−60] chemical processes. Consequently, there is a large interest in the optimization of its performance, a goal for which a profound mechanistic understanding of *how* the process occurs at the microscopic level is essential.[61,62] While the nature of the metal center (with rhodium and cobalt being the most common ones) is paramount, the importance of the

https://doi.org/10.1021/acscatal.5c00348
ACS Catal. 2025, 15, 4739−4745

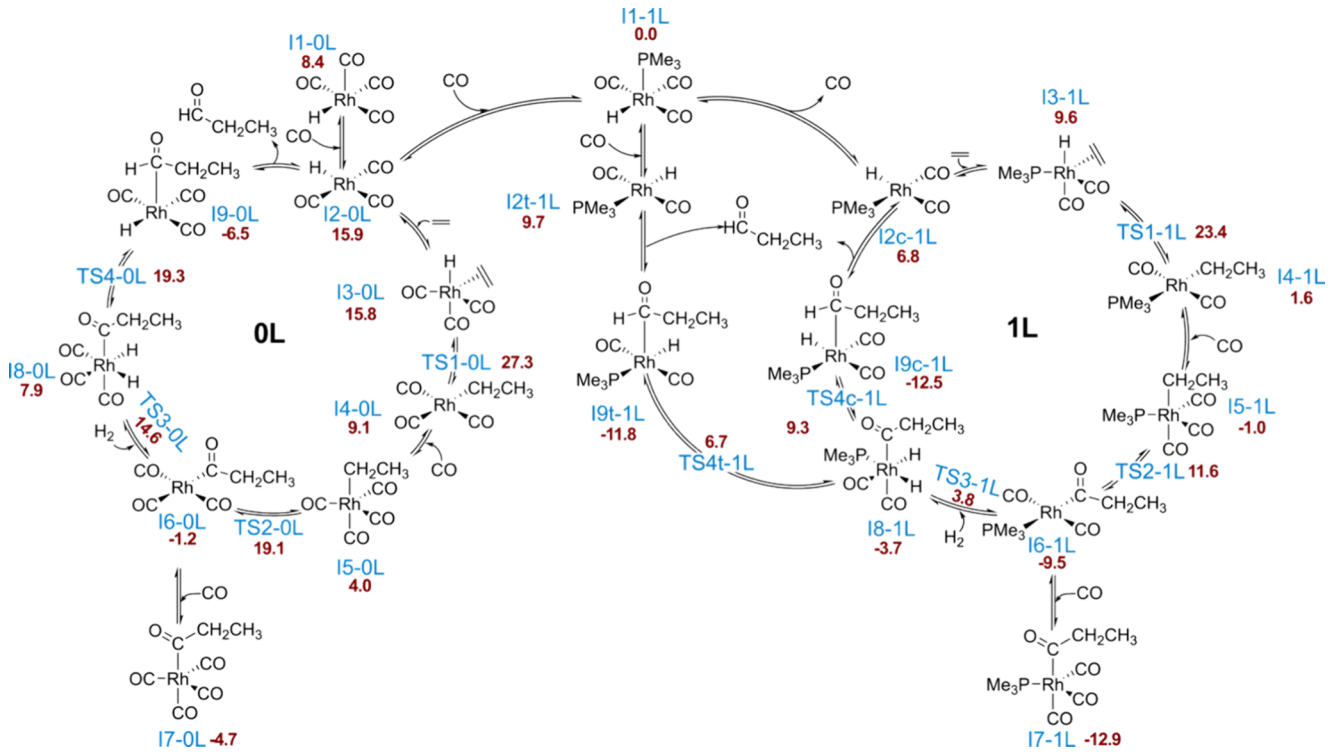

Figure 3. Chemical reaction network for hydroformylation (ΔG^0 = −25.9 kcal mol^{-1}) with the Rh-carbonyl complex (**0L**, left) and the monosubstituted trimethylphosphine derivative (**1L**, right). In burgundy, relative Gibbs free energies were at 350.0 K and 1.0 M, with I1-1L as a reference.

ligands in modulating the reactivity of the complex cannot be underestimated. Herein, as a foundational study, we decided to select an Rh-based complex with two of the simplest ligands: carbonyl and trimethylphosphine. In this way, we were able to focus on determining the influence of ligand exchange processes in catalytic performance, considering the catalytic cycles with zero (**0L**) and one (**1L**) phosphine ligands in the rhodium carbonyl hydride catalyst. While further substitution might be possible (**2L** and **3L** analogues), we considered the simplified system to limit the computational cost, as the number of reactions and therefore the complexity of the underlying microkinetic simulations will skyrocket for the full picture. Nonetheless, it shall be noted that the use of this model system limits us from direct comparison with experimental data, which are not directly available. We characterized the reaction mechanism starting from the proposal from Sparta and co-workers,[63] with the further consideration of the cis/trans isomerism arising in the monosubstituted catalyst (**1L**), depending on the relative positions of the hydrogen atom and phosphine ligand.

As depicted in Figure 3, we considered the exchange to happen via the active catalytic species I2-0L capturing PMe_3 to form I1-1L, which then leads to the also active I2c-1L by releasing CO. In this framework, we regarded the axial—equatorial ligand repositioning happening in I1 bipyramidal derivatives via Berry pseudorotation to be fast, as stated in the literature.[64]

From this mechanistic proposal, we defined the corresponding set of chemical reactions, their reaction energies, and corresponding Gibbs free energy barriers, considering 350 K as the working temperature and a 1.0 M reference state for all species in the reaction network. Although this temperature is above the boiling point of PMe_3 and thus will not be feasible on an experimental setup, it provides a fast enough reaction to explore the behavior of our model system: as aforementioned, direct comparison with experimental results would require to test alternative, more complex ligands. All barrierless processes were assumed to be diffusion-controlled,[31] with a constant barrier of 4.0 kcal mol^{-1}. From there, we set up initial concentrations for all reactants and for the catalyst: $[\mathbf{H_2}] = [\mathbf{CO}] = [\mathbf{C_2H_4}] = \mathbf{0.05\ M}$ and $[\mathbf{Rh}] = \mathbf{5 \times 10^{-4}\ M}$. To explore the influence of the phosphine additive, we tested a range of values from 0 to 1.0 M (considering a logarithmic scale starting at $\log[PMe_3] = -10$) and ran simulations of 10^5 s (≈28 h).

Figure 4 showcases the crucial effect that ligand exchange has on the efficacy of the overall hydroformylation process. When more phosphine is available, as expected, the **1L** cycle is activated, becoming the main form of the catalyst at $[PMe_3] \geq 1 \times 10^{-3}$ M. A deeper exploration of the specific catalyst states is shown in the Supporting Information (Figure S3). Throughout this process, the reaction becomes much faster, with the time spent until reaching a 99% conversion lowering from approximately 6 h (with the "pure" **0L** cycle, in the left part of the plot) to around only 1.5 h. The transition region is particularly interesting, highlighting how in the range 10^{-4} M $\leq [PMe_3] \leq 10^{-2}$ M both cycles are operative, and therefore, the net process starts becoming more efficient even with the catalyst not yet being completely transformed.

At this point, we aimed to gain deeper insight into how the reactivity switch from the **0L** to the **1L** cycle was taking place. To this end, we analyzed the degree of rate control (DRC) of all reactions in the network across our range of initial PMe_3 concentration values, determining how the rate-determining step changed throughout the process. To compute the DRC, we considered a simple finite difference approach,[65,66] applying

https://doi.org/10.1021/acscatal.5c00348
ACS Catal. 2025, 15, 4739−4745

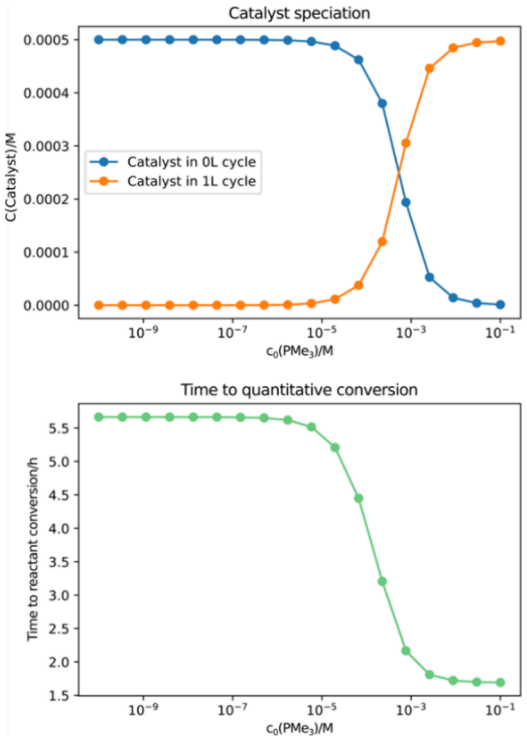

Figure 4. Catalyst distribution at t = 1h (above) and time required to reach a 99% ethylene conversion (below). X-axis is the initial concentration of phosphine, on a logarithmic scale.

0.01 kcal mol^{-1} perturbations to all barriers and computing the rates for aldehyde formation:

$$\mathrm{DRC}_i = \frac{k_i}{r}\frac{\delta r_i}{\delta k_i} \approx \frac{k_i}{r}\frac{\Delta r}{\Delta k_i}$$

where k_i is the rate constant for the i-th reaction, r is the overall reaction rate (aldehyde formation), and Δr and Δk_i are the computed differences in the overall rate and the rate constant, respectively, after the perturbation is applied to the i-th reaction.

To ensure reaction rates to be stable, we set up a low concentration of catalyst [**Rh**] = $\mathbf{10^{-6}}$ **M** and a shorter simulation time (10^4 s) for these runs, where we consider a differential reactor (very low conversion regime) to ensure the consistency of reaction rates (ref 52).

From Figure 5, we clearly observe the switch between the **0L** cycle governed by the formation of aldehyde ($I_8 - 0L \rightleftharpoons I_9 - 0L$) and the **1L** one, where the rate-determining step is the insertion of ethylene ($I_3 - 1L \rightleftharpoons I_4 - 1L$). In the transition region, the equivalent ethylene insertion/β-hydride elimination ($I_3 - 0L \rightleftharpoons I_4 - 0L$) has a negative DRC, implying that it is *hindering* global product formation. As this process is the rate-determining step of the **0L** cycle and that at this concentration of phosphine both cycles are coexisting, this reaction is blocking the more productive catalytic cycle **1L** and trapping the catalyst, making aldehyde production less effective.

Furthermore, we can also inspect the *apparent activation energies* of these reactions, considering simulations in a range of temperatures (for instance from 325.0 to 375.0 K) and an Arrhenius-like law, extracting an apparent activation energy E_a^{app} from the slope.

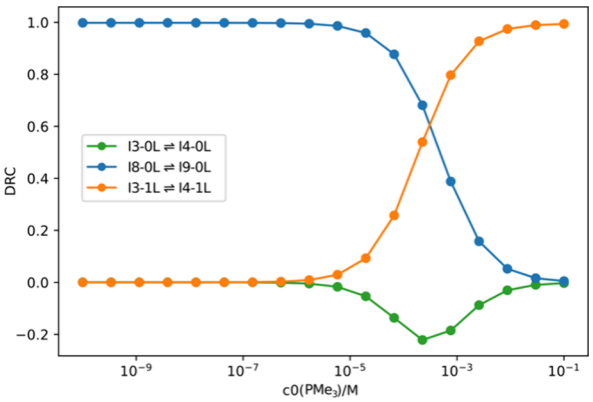

Figure 5. Degree of rate control (DRC) against the initial phosphine concentration (X-axis) for the most influential processes in the reaction network.

$$\ln r = -\frac{E_a^{app}}{R}\cdot\frac{1}{T} + \ln A$$

where r is the rate constant and A is the pre-exponential rate from Arrhenius' law. Figure 6 shows an upward trend in both

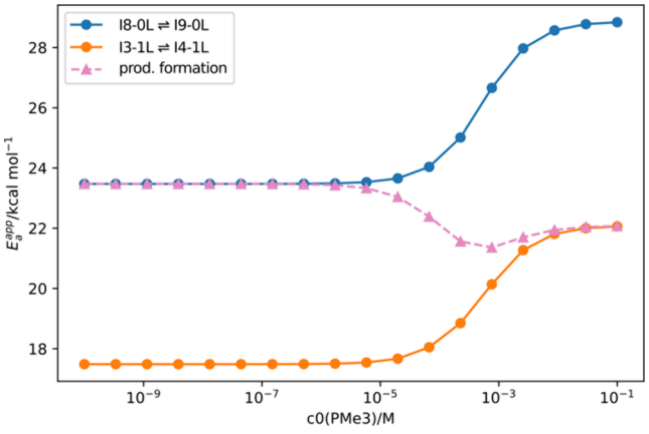

Figure 6. Apparent activation energies of rate-determining steps of **0L** (blue, circles) and **1L** (orange, circles) cycles, as well as for the net formation of propenal (pink, triangles) in kcal mol^{-1}, against initial phosphine concentration (X-axis).

activation energies: the presence of larger quantities of phosphine (from around 1.0×10^{-4} M, 2 orders of magnitude above the catalyst concentration) hampers the overall kinetics of both processes. Nonetheless, the switch from the less favored **0L** cycle to the **1L** cycle implies a net acceleration of the underlying process, as observed in Figure 4. Moreover, the poisoning effect of ethylene insertion in **0L**, from the DRCs in Figure 5, also influences the reactivity in the transition region, dampening the acceleration of the reaction. Looking at the net rate for product formation and in line with these findings, we observe a net decrease of the activation barrier from 23.5 to around 22.0 kcal mol^{-1} as the concentration of phosphine increases: the formation of the aldehyde clearly switches from being driven by the **0L** cycle, matching the apparent activation energy of this subsystem, to do the same for the **1L** cycle. The 0.5 kcal mol^{-1} gap arising between the minimum E_a at [PMe_3] = $1.0 \cdot 10^{-3}$ M and the pure **1L**-operating situation at larger phosphine concentrations might be related to the increase of activation energies for the rate-determining steps showcased in

https://doi.org/10.1021/acscatal.5c00348
ACS Catal. 2025, 15, 4739−4745

Figure 6. Nevertheless, this small shift does not affect the longer-time scale reactivity observed with larger catalyst concentrations, as previously discussed for Figure 4.

All in all, our approach provides an in-depth explanation of the catalytic activity of Rh-based catalysts for hydroformylation. Both the long- and short-time scale results agree with the expected behavior of this widely studied system: the increased efficacy of the phosphine-substituted analogue against the Rh-carbonyl complex. Moreover, we identify several specific aspects that are also known to happen in hydroformylation processes, such as the appearance of the bipyramidal I1-1L intermediate as a resting state or how the presence of phosphine stabilizes the catalyst and limits the extent of self-poisoning by excess CO (formation of I7).

CONCLUSIONS AND OUTLOOK

In this work, we introduce MicroKatc, a new automated platform to perform in-depth analysis of complex reaction networks and catalytic cycles using microkinetic simulations. Through this tool, we simplify the setup of the simulations from computational results (Gibbs free energies and mechanism definitions), streamlining the production of simulations in ranges of temperatures or initial concentrations of ligands and catalyst. Additionally, we provide tools to easily explore the degree of rate control or the apparent activation energy. We believe that these are valuable tools in computational catalysis that have been underutilized in the homogeneous realm.

Regarding the case study on hydroformylation, we provide novel insights into the reactivity switch happening upon the addition of a ligand (trimethylphosphine) to a Rh-carbonyl catalyst. Our findings demonstrate the increased efficacy of the phosphine-bearing catalytic cycle **1L**, its degree of formation, as well as the rate-determining steps in the intricate reaction mechanism. Consequently, together with the development of MicroKatc, this study paves the way for future extensions where, for instance, different ligands might be compared.

Computational Details. All DFT calculations were carried out with Gaussian16[67] (revision A.03) with the ωB97X-D[68] functional and a def2-TZVP[69,70] basis set, using the SDD[71,72] pseudopotential for Rh atoms and the SMD implicit solvent model[73] with parameters for toluene. All species were characterized with unconstrained geometry optimizations, and harmonic frequency analysis was used to determine the nature of the minima and transition states. All calculations are available as a data set collection in the ioChem-BD[74] platform and can be accessed through the following link: doi.org/10.19061/iochem-bd-1-345.

Regarding microkinetic simulations, the LSODA deterministic solver was employed in all cases, with tolerances of 10^{-14} (relative) and 10^{-16} (absolute) to ensure numeric stability. Gibbs free energies were computed at the corresponding working temperatures (350.0 K, except for the apparent activation energy analysis where the whole range was used), assuming a 1.0 M standard state. The MicroKatc source code is available in a GitHub repository,[75] as well as a release in Zenodo (DOI: 10.5281/zenodo.14881305).

ASSOCIATED CONTENT

Supporting Information

The Supporting Information is available free of charge at https://pubs.acs.org/doi/10.1021/acscatal.5c00348.

Geometries and energies of computed structures, reaction barriers and rate constants, DFT functional selection, exploration of catalyst state, thermodynamic degree of rate control (TRC), and additional references (PDF)

AUTHOR INFORMATION

Corresponding Authors

Diego Garay-Ruiz − *Institute of Chemical Research of Catalonia (ICIQ), The Barcelona Institute of Science and Technology (BIST), Tarragona 43007, Spain;* orcid.org/0000-0003-0744-0562; Email: dgarayru@gmail.com

Carles Bo − *Institute of Chemical Research of Catalonia (ICIQ), The Barcelona Institute of Science and Technology (BIST), Tarragona 43007, Spain; Department of Physical and Inorganic Chemistry, University Rovira i Virgili (URV), Tarragona 43007, Spain;* orcid.org/0000-0001-9581-2922; Email: cbo@iciq.cat

Authors

Orkhan Abdullayev − *Institute of Chemical Research of Catalonia (ICIQ), The Barcelona Institute of Science and Technology (BIST), Tarragona 43007, Spain*

Berta Bori-Bru − *Institute of Chemical Research of Catalonia (ICIQ), The Barcelona Institute of Science and Technology (BIST), Tarragona 43007, Spain*

Complete contact information is available at: https://pubs.acs.org/10.1021/acscatal.5c00348

Author Contributions

All authors have given approval to the final version of the manuscript.

Notes

The authors declare no competing financial interest.

ACKNOWLEDGMENTS

We gratefully acknowledge the Spanish Ministry of Science and Innovation MCIN/AEI/10.13039/501100011033 for project PID2020-112806RB-I00 and CEX2019-000925-S, the European Union NextGenerationEU/PRTR (TED2021-132850B−I00), the ICIQ Foundation, and the CERCA program of the Generalitat de Catalunya for funding. We also thank Dr. A. Sabadell-Rendón for valuable discussion and feedback.

REFERENCES

(1) Fey, N. The Contribution of Computational Studies to Organometallic Catalysis: Descriptors. *Mechanisms and Models. Dalton Trans* **2010**, *39* (2), 296−310.

(2) Sperger, T.; Sanhueza, I. A.; Kalvet, I.; Schoenebeck, F. Computational Studies of Synthetically Relevant Homogeneous Organometallic Catalysis Involving Ni, Pd, Ir, and Rh: An Overview of Commonly Employed DFT Methods and Mechanistic Insights. *Chem. Rev.* **2015**, *115* (17), 9532−9586.

(3) Santoro, S.; Kalek, M.; Huang, G.; Himo, F. Elucidation of Mechanisms and Selectivities of Metal-Catalyzed Reactions Using Quantum Chemical Methodology. *Acc. Chem. Res.* **2016**, *49* (5), 1006−1018.

(4) Funes-Ardoiz, I.; Schoenebeck, F. Established and Emerging Computational Tools to Study Homogeneous Catalysis—From Quantum Mechanics to Machine Learning. *Chem.* **2020**, *6* (8), 1904−1913.

(5) Qiao, C.; Villar-Yanez, A.; Sprachmann, J.; Limburg, B.; Bo, C.; Kleij, A. W. Organocatalytic Trapping of Elusive Carbon Dioxide

Based Heterocycles by a Kinetically Controlled Cascade Process. *Angew. Chem.* **2020**, *132* (42), 18604−18609.
(6) Sterling, A. J.; Zavitsanou, S.; Ford, J.; Duarte, F. Selectivity in Organocatalysis—From Qualitative to Quantitative Predictive Models. *WIREs Comput. Mol. Sci.* **2021**, *11* (5), No. e1518.
(7) Luo, C.; Alegre-Requena, J. V.; Sujansky, S. J.; Pajk, S. P.; Gallegos, L. C.; Paton, R. S.; Bandar, J. S. Mechanistic Studies Yield Improved Protocols for Base-Catalyzed Anti-Markovnikov Alcohol Addition Reactions. *J. Am. Chem. Soc.* **2022**, *144* (22), 9586−9596.
(8) Norjmaa, G.; Ujaque, G.; Lledós, A. Beyond Continuum Solvent Models in Computational Homogeneous Catalysis. *Top. Catal.* **2022**, *65* (1−4), 118−140.
(9) Fey, N.; Lynam, J. M. Computational Mechanistic Study in Organometallic Catalysis: Why Prediction Is Still a Challenge. *WIREs Comput. Mol. Sci.* **2022**, *12* (4), No. e1590.
(10) Laplaza, R.; Das, S.; Wodrich, M. D.; Corminboeuf, C. Constructing and Interpreting Volcano Plots and Activity Maps to Navigate Homogeneous Catalyst Landscapes. *Nat. Protoc.* **2022**, *17* (11), 2550−2569.
(11) Ulissi, Z. W.; Medford, A. J.; Bligaard, T.; Nørskov, J. K. To Address Surface Reaction Network Complexity Using Scaling Relations Machine Learning and DFT Calculations. *Nat. Commun.* **2017**, *8* (1), 14621.
(12) Comas-Vives, A.; Larmier, K.; Copéret, C. Understanding Surface Site Structures and Properties by First Principles Calculations: An Experimental Point of View! *Chem. Commun.* **2017**, *53* (31), 4296−4303.
(13) Chen, B. W. J.; Xu, L.; Mavrikakis, M. Computational Methods in Heterogeneous Catalysis. *Chem. Rev.* **2021**, *121* (2), 1007−1048.
(14) Frei, M. S.; Mondelli, C.; García-Muelas, R.; Morales-Vidal, J.; Philipp, M.; Safonova, O. V.; López, N.; Stewart, J. A.; Ferré, D. C.; Pérez-Ramírez, J. Nanostructure of Nickel-Promoted Indium Oxide Catalysts Drives Selectivity in CO2 Hydrogenation. *Nat. Commun.* **2021**, *12* (1), 1960.
(15) Pablo-García, S.; Veenstra, F. L. P.; Ting, L. R. L.; García-Muelas, R.; Dattila, F.; Martín, A. J.; Yeo, B. S.; Pérez-Ramírez, J.; López, N. Mechanistic Routes toward C3 Products in Copper-Catalysed CO2 Electroreduction. *Catal. Sci. Technol.* **2022**, *12* (2), 409−417.
(16) Martínez-Núñez, E. An Automated Method to Find Transition States Using Chemical Dynamics Simulations. *J. Comput. Chem.* **2015**, *36* (4), 222−234.
(17) Maeda, S.; Harabuchi, Y.; Takagi, M.; Taketsugu, T.; Morokuma, K. Artificial Force Induced Reaction (AFIR) Method for Exploring Quantum Chemical Potential Energy Surfaces. *Chem. Rec.* **2016**, *16* (5), 2232−2248.
(18) Kim, Y.; Kim, J. W.; Kim, Z.; Kim, W. Y. Efficient Prediction of Reaction Paths through Molecular Graph and Reaction Network Analysis. *Chem. Sci.* **2018**, *9* (4), 825−835.
(19) Guan, Y.; Ingman, V. M.; Rooks, B. J.; Wheeler, S. E. AARON: An Automated Reaction Optimizer for New Catalysts. *J. Chem. Theory Comput.* **2018**, *14* (10), 5249−5261.
(20) Martínez-Núñez, E.; Barnes, G. L.; Glowacki, D. R.; Kopec, S.; Peláez, D.; Rodríguez, A.; Rodríguez-Fernández, R.; Shannon, R. J.; Stewart, J. J. P.; Tahoces, P. G.; Vazquez, S. A. AutoMeKin2021: An Open-source Program for Automated Reaction Discovery. *J. Comput. Chem.* **2021**, *42* (28), 2036−2048.
(21) Hashemi, A.; Bougueroua, S.; Gaigeot, M.-P.; Pidko, E. A. ReNeGate: A Reaction Network Graph-Theoretical Tool for Automated Mechanistic Studies in Computational Homogeneous Catalysis. *J. Chem. Theory Comput.* **2022**, *18* (12), 7470−7482.
(22) Maeda, S.; Harabuchi, Y.; Hayashi, H.; Mita, T. Toward Ab Initio Reaction Discovery Using the Artificial Force Induced Reaction Method. *Annu. Rev. Phys. Chem.* **2023**, *74* (1), 287−311.
(23) Kozuch, S.; Shaik, S. How to Conceptualize Catalytic Cycles? The Energetic Span Model. *Acc. Chem. Res.* **2011**, *44* (2), 101−110.
(24) Kozuch, S. A Refinement of Everyday Thinking: The Energetic Span Model for Kinetic Assessment of Catalytic Cycles. *Wiley Interdiscip. Rev. Comput. Mol. Sci.* **2012**, *2* (5), 795−815.
(25) Kozuch, S. Steady State Kinetics of Any Catalytic Network: Graph Theory, the Energy Span Model, the Analogy between Catalysis and Electrical Circuits, and the Meaning of "Mechanism. *ACS Catal.* **2015**, *5* (9), 5242−5255.
(26) Garay-Ruiz, D.; Bo, C. Revisiting Catalytic Cycles: A Broader View through the Energy Span Model. *ACS Catal.* **2020**, *10* (21), 12627−12635.
(27) Goldsmith, C. F.; West, R. H. Automatic Generation of Microkinetic Mechanisms for Heterogeneous Catalysis. *J. Phys. Chem. C* **2017**, *121* (18), 9970−9981.
(28) Baz, A.; Dix, S. T.; Holewinski, A.; Linic, S. Microkinetic Modeling in Electrocatalysis: Applications, Limitations, and Recommendations for Reliable Mechanistic Insights. *J. Catal.* **2021**, *404*, 864−872.
(29) Motagamwala, A. H.; Dumesic, J. A. Microkinetic Modeling: A Tool for Rational Catalyst Design. *Chem. Rev.* **2021**, *121* (2), 1049−1076.
(30) Pablo-García, S.; Sabadell-Rendón, A.; Saadun, A. J.; Morandi, S.; Pérez-Ramírez, J.; López, N. Generalizing Performance Equations in Heterogeneous Catalysis from Hybrid Data and Statistical Learning. *ACS Catal.* **2022**, *12* (2), 1581−1594.
(31) Besora, M.; Maseras, F. Microkinetic Modeling in Homogeneous Catalysis. *Wiley Interdiscip. Rev. Comput. Mol. Sci.* **2018**, *8* (6), 1−13.
(32) Pérez-Soto, R.; Besora, M.; Maseras, F. The Challenge of Reproducing with Calculations Raw Experimental Kinetic Data for an Organic Reaction. *Org. Lett.* **2020**, *22* (8), 2873−2877.
(33) Sciortino, G.; Maseras, F. Microkinetic Modelling in Computational Homogeneous Catalysis and Beyond. *Theor. Chem. Acc.* **2023**, *142* (10), 99.
(34) Petrus, E.; Garay-Ruiz, D.; Reiher, M.; Bo, C. Multi-Time-Scale Simulation of Complex Reactive Mixtures: How Do Polyoxometalates Form? *J. Am. Chem. Soc.* **2023**, *145* (34), 18920−18930.
(35) Díaz-Ruiz, M.; Nieto-Rodríguez, M.; Maseras, F. Revealing the Mechanistic Features of an Electrosynthetic Catalytic Reaction and the Role of Redox Mediators through DFT Calculations and Microkinetic Modeling. *ChemPhysChem* **2024**, *25* (15), No. e202400402.
(36) Rama, R. J.; Nova, A.; Nicasio, M. C. Microkinetic Model as a Crucial Tool for Understanding Homogeneous Catalysis. *ChemCatChem.* **2024**, *16*, No. e202400224.
(37) Worakul, T.; Laplaza, R.; Das, S.; Wodrich, M. D.; Corminboeuf, C. Microkinetic Molecular Volcano Plots for Enhanced Catalyst Selectivity and Activity Predictions. *ACS Catal.* **2024**, *14* (13), 9829−9839.
(38) Tolman, C. A. Steric Effects of Phosphorus Ligands in Organometallic Chemistry and Homogeneous Catalysis. *Chem. Rev.* **1977**, *77* (3), 313−348.
(39) Van Leeuwen, P. W. N. M. *Homogeneous Catalysis: Understanding the Art*; Kluwer Scientific Publishers: The Netherlands, Dordrecht, 2004. .
(40) Gorin, D. J.; Sherry, B. D.; Toste, F. D. Ligand Effects in Homogeneous Au Catalysis. *Chem. Rev.* **2008**, *108* (8), 3351−3378.
(41) De Azambuja, F.; Lenie, J.; Parac-Vogt, T. N. Homogeneous Metal Catalysts with Inorganic Ligands: Probing Ligand Effects in Lewis Acid Catalyzed Direct Amide Bond Formation. *ACS Catal.* **2021**, *11* (1), 271−277.
(42) Bayón, J. C.; Claver, C.; Masdeu-Bultó, A. M. Homogeneous Catalysis with Transition Metal Complexes Containing Sulfur Ligands. *Coord. Chem. Rev.* **1999**, *193*−*195*, 73−145.
(43) De Vries, J. G.; De Vries, A. H. M. The Power of High-Throughput Experimentation in Homogeneous Catalysis Research for Fine Chemicals. *Eur. J. Org. Chem.* **2003**, *34* (24), No. chin.200324228.
(44) Renom-Carrasco, M.; Lefort, L. Ligand Libraries for High Throughput Screening of Homogeneous Catalysts. *Chem. Soc. Rev.* **2018**, *47* (13), 5038−5060.
(45) Fey, N. Lost in Chemical Space? Maps to Support Organometallic Catalysis. *Chem. Cent. J.* **2015**, *9* (1), 38.

https://doi.org/10.1021/acscatal.5c00348
ACS Catal. 2025, 15, 4739−4745

(46) Hueffel, J. A.; Sperger, T.; Funes-Ardoiz, I.; Ward, J. S.; Rissanen, K.; Schoenebeck, F. Accelerated Dinuclear Palladium Catalyst Identification through Unsupervised Machine Learning. *Science* **2021**, *374* (6571), 1134−1140.
(47) Hashemi, A.; Bougueroua, S.; Gaigeot, M.-P.; Pidko, E. A. HiREX: High-Throughput Reactivity Exploration for Extended Databases of Transition-Metal Catalysts. *J. Chem. Inf. Model.* **2023**, *63* (19), 6081−6094.
(48) Hirst, J. D.; Boobier, S.; Coughlan, J.; Streets, J.; Jacob, P. L.; Pugh, O.; Özcan, E.; Woodward, S. ML Meets MLn: Machine Learning in Ligand Promoted Homogeneous Catalysis. *Artif. Intell. Chem.* **2023**, *1* (2), No. 100006.
(49) Kalikadien, A. V.; Mirza, A.; Hossaini, A. N.; Sreenithya, A.; Pidko, E. A. Paving the Road towards Automated Homogeneous Catalyst Design. *ChemPlusChem.* **2024**, *89* (7), No. e202300702.
(50) Garay-Ruiz, D. *gTOFfee*. GitLab Repository. https://gitlab.com/dgarayr/gtoffee (accessed 2022−08−26).
(51) Chacko, R.; Gossler, H.; Angeli, S.; Deutschmann, O. Interconnected Digital Solutions to Accelerate Modeling of the Reaction Kinetics in Catalysis. *ChemCatChem.* **2024**, *16*, No. e202301355.
(52) Sabadell-Rendón, A.; Kaźmierczak, K.; Morandi, S.; Euzenat, F.; Curulla-Ferré, D.; López, N. Automated MUltiscale Simulation Environment. *Digit. Discovery* **2023**, *2* (6), 1721−1732.
(53) Garay-Ruiz, D. *thermochange*. GitLab Repository. https://gitlab.com/dgarayr/copasi-helper (accessed 2024−08−30).
(54) Hoops, S.; Sahle, S.; Gauges, R.; Lee, C.; Pahle, J.; Simus, N.; Singhal, M.; Xu, L.; Mendes, P.; Kummer, U. COPASI—a COmplex PAthway SImulator. *Bioinformatics* **2006**, *22* (24), 3067−3074.
(55) Garay-Ruiz, D. *copasi-helper*. GitLab Repository. https://gitlab.com/dgarayr/copasi-helper (accessed 2024−08−30).
(56) Mao, Z.; Campbell, C. T. Apparent Activation Energies in Complex Reaction Mechanisms: A Simple Relationship via Degrees of Rate Control. *ACS Catal.* **2019**, *9* (10), 9465−9473.
(57) Kamer, P. C. J.; Reek, J. N. H.; van Leeuwen, P. W. N. M. Rhodium Catalyzed Hydroformylation; In *Mechanisms in Homogeneous Catalysis: A Spectroscopic Approach* Van Leeuwen, P. W. N. M.; Claver, C., Eds.; Catalysis by Metal Complexes; Springer: Netherlands, Dordrecht, 2005; Vol. *22*. .
(58) Rush, L. E.; Pringle, P. G.; Harvey, J. N. Computational Kinetics of Cobalt-Catalyzed Alkene Hydroformylation. *Angew. Chem. - Int. Ed.* **2014**, *53* (33), 8672−8676.
(59) Stanley, G. G. Hydroformylation (OXO) Catalysis. In *Kirk-Othmer Encyclopedia of Chemical Technology*; John Wiley & Sons, Inc. 2017; pp 1−19. .
(60) Hood, D. M.; Johnson, R. A.; Carpenter, A. E.; Younker, J. M.; Vinyard, D. J.; Stanley, G. G. Highly Active Cationic Cobalt(II) Hydroformylation Catalysts. *Science* **2020**, *367* (6477), 542−548.
(61) Siradze, S.; Poissonnier, J.; Frøseth, M.; Stensrød, R. E.; Heyn, R. H.; Thybaut, J. W. Kinetics Assessment of the Homogeneously Catalyzed Hydroformylation of Ethylene on an Rh Catalyst. *Ind. Eng. Chem. Res.* **2021**, *60* (46), 16665−16681.
(62) Zong, Y.; Zhang, R.; Ma, B.; Peng, J.; Wu, C.; Zou, X.; Qian, Y.; Chen, G.-Q.; Zhang, X. Robust, Scalable, and Highly Selective Spirocyclic Catalysts for Industrial Hydroformylation and Isomerization-Hydroformylation. *Sci. Adv.* **2024**, *10* (29), No. eado9607.
(63) Sparta, M.; Børve, K. J.; Jensen, V. R. Activity of Rhodium-Catalyzed Hydroformylation: Added Insight and Predictions from Theory. *J. Am. Chem. Soc.* **2007**, *129* (27), 8487−8499.
(64) Koga, N.; Jin, S. Q.; Morokuma, K. Rearrangement through Berry Pseudorotation and Olefin Insertion of D8 Five-Coordinate Rh(H)(C2H4)(CO)2(PH3). An Ab Initio MO Study. *J. Am. Chem. Soc.* **1988**, *110* (11), 3417−3425.
(65) Campbell, C. T. Finding the Rate-Determining Step in a Mechanism. *J. Catal.* **2001**, *204* (2), 520−524.
(66) Yang, Y.; Achar, S. K.; Kitchin, J. R. Evaluation of the Degree of Rate Control via Automatic Differentiation. *AIChE J.* **2022**, *68* (6), No. e17653.
(67) Frisch, M. J.; Trucks, G. W.; Schlegel, H. B.; Scuseria, G. E.; Robb, M. A.; Cheeseman, J. R.; Scalmani, G.; Barone, V.; Mennucci, B.; Petersson, G. A.; Nakatsuji, H.; Caricato, M.; Li, X.; Hratchian, H. P.; Izmaylov, A. F.; Bloino, J.; Zheng, G.; Sonnenberg, J. L.; Hada, M.; Ehara, M.; Toyota, K.; Fukuda, R.; Hasegawa, J.; Ishida, M.; Nakajima, T.; Honda, Y.; Kitao, O.; Nakai, H.; Vreven, T.; Montgomery, J. A., Jr.; Peralta, J. E.; Ogliaro, F.; Bearpark, M.; Heyd, J. J.; Brothers, E.; Kudin, K. N.; Staroverov, V. N.; Kobayashi, R.; Normand, J.; Raghavachari, K.; Rendell, A.; Burant, J. C.; Iyengar, S. S.; Tomasi, J.; Cossi, M.; Rega, N.; Millam, J. M.; Klene, M.; Knox, J. E.; Cross, J. B.; Bakken, V.; Adamo, C.; Jaramillo, J.; Gomperts, R.; Stratmann, R. E.; Yazyev, O.; Austin, A. J.; Cammi, R.; Pomelli, C.; Ochterski, J. W.; Martin, R. L.; Morokuma, K.; Zakrzewski, V. G.; Voth, G. A.; Salvador, P.; Dannenberg, J. J.; Dapprich, S.; Daniels, A. D.; Farkas, O.; Foresman, J. B.; Ortiz, J. V.; Cioslowski, J.; Fox, D. J. *Gaussian09* Revision D.01, Gaussian Inc.: Wallingford CT, 2010.
(68) Chai, J. D.; Head-Gordon, M. Long-Range Corrected Hybrid Density Functionals with Damped Atom-Atom Dispersion Corrections. *Phys. Chem. Chem. Phys.* **2008**, *10* (44), 6615−6620.
(69) Weigend, F.; Ahlrichs, R. Balanced Basis Sets of Split Valence, Triple Zeta Valence and Quadruple Zeta Valence Quality for H to Rn: Design and Assessment of Accuracy. *Phys. Chem. Chem. Phys.* **2005**, *7* (18), 3297−3305.
(70) Weigend, F. Accurate Coulomb-Fitting Basis Sets for H to Rn. *Phys. Chem. Chem. Phys.* **2006**, *8* (9), 1057.
(71) Fuentealba, P.; Preuss, H.; Stoll, H.; Von Szentpály, L. A Proper Account of Core-Polarization with Pseudopotentials: Single Valence-Electron Alkali Compounds. *Chem. Phys. Lett.* **1982**, *89* (5), 418−422.
(72) Dolg, M.; Wedig, U.; Stoll, H.; Preuss, H. Energy-Adjusted Ab Initio Pseudopotentials for the First Row Transition Elements. *J. Chem. Phys.* **1987**, *86* (2), 866−872.
(73) Marenich, A. V.; Cramer, C. J.; Truhlar, D. G. Universal Solvation Model Based on Solute Electron Density and on a Continuum Model of the Solvent Defined by the Bulk Dielectric Constant and Atomic Surface Tensions. *J. Phys. Chem. B* **2009**, *113* (18), 6378−6396.
(74) Álvarez-Moreno, M.; De Graaf, C.; López, N.; Maseras, F.; Poblet, J. M.; Bo, C. Managing the Computational Chemistry Big Data Problem: The ioChem-BD Platform. *J. Chem. Inf. Model.* **2015**, *55* (1), 95−103.
(75) Abdullayev, O. *MicroKatc*. GitHub Repository. https://github.com/0rkhann/MicroKatc (accessed 2024−10−21).

https://doi.org/10.1021/acscatal.5c00348
ACS Catal. 2025, 15, 4739−4745